PHOTOMASK

BACUS—The international technical group of SPIE dedicated to the advancement of photomask technology.

Best Poster — Photomask Japan 2018

Intra-field mask-to-mask overlay, separating the mask writing from the dynamic pellicle contribution

Richard van Haren, Orion Mouraille, Leon van Dijk, and Ronald Otten, ASML, Flight Forum 1900 (no. 5846), 5657 EZ Eindhoven, The Netherlands

Steffen Steinert and Dirk Beyer, Carl Zeiss SMT GmbH, Carl-Zeiss-Promenade 10, 07745 Jena, Germany

Koen D'havé, IMEC, Kapeldreef 75, B-30001, Leuven, Belgium

ABSTRACT

The number of masks required to produce an integrated circuit has increased tremendously over the past years. The main reason for this is that a single layer mask exposure and etch was no longer sufficient to meet the required pattern density. A solution was found in the application of multi-patterning steps, including multiple masks, before the final pattern is transferred into the underlying substrate. Consequently, the mask-to-mask contribution as part of the overall on-product (intra-layer) overlay budget could not be neglected anymore. While the tight on-product overlay specifications (< 3-nm) were initially only requested for the intra-layer (e.g. multi Litho Etch Litho Etch) overlay performance, recently these tight requirements are also imposed for the layer-to-layer overlay.

Recently, we reported on an extensive study in which the mask-to-mask overlay contribution as determined by the PROVE® mask registration tool was correlated with actual on-wafer measurements. Two ASML BMMO (Baseliner Matched Machine Overlay) masks were used for this purpose. Initially, no pellicles were mounted onto the masks. An excellent correlation was found between the measurements on the PROVE® tool and the on-wafer results reaching $R^2 > 0.96$ with an accuracy of 0.58-nm. The accuracy level can be further improved since all underlying contributors were identified. It was concluded that the expected overlay as measured on-wafer can be fully determined by off-line registration measurements only.

An important note is that the off-line registration measurements on the PROVE® tool are performed in a static mode, while the exposures on an ASML TWINSCAN™ are performed in a dynamic (scanning) mode. No impact was observed since both masks were not equipped with a pellicle. One can expect that also for the case where *both* masks are equipped with a pellicle of the same type, the impact is negligible. The reason for this is that all pellicle induced errors are likely to be the same for both masks in scanning mode and will cancel out in the overlay. However, the

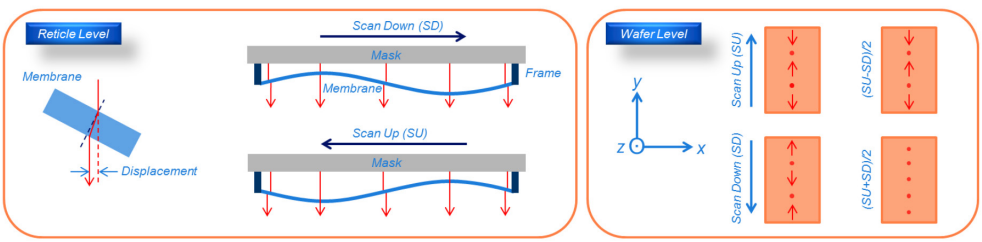

Figure 1. A deformed pellicle membrane during scan. The thin membrane acts as plan-parallel plate causing a displacement shift due to Snell's law. The displacement depends on the local angle, the thickness, and the refractive index of the membrane used. In case the scan properties are completely symmetric, one may expect that the resulting intra-field distortion fingerprint changes sign when considering scan-up and scan-down fields.

BACUS NEWS

JULY 2018
VOLUME 34, ISSUE 7

SPIE.

10807-17

EDITORIAL

Cloud Computing – An Option for Mask Data Prep?

Bala Thumma, Synopsys, Inc.

As technology advances, manufacturing ICs and the associated masks is becoming ever more challenging and costly. This is not only true for the semiconductor industry, but also for the software vendors. Software must now process several TB of data per mask layer, in a limited amount of time, say 8 to 12 hours in a mask shop or wafer fab. The only way to achieve this is to leverage massively parallel processing of data. This implies breaking a large problem into smaller ones and distributing the work over many CPUs and servers. The end customer may run the software on several thousand CPUs to achieve the required turnaround time. This in turn requires a decently sized server farm depending on the complexity of the data, with which come the associated costs of hardware, space, power, and managing the hardware and human resources. This cost can become prohibitive at some point, bringing us to the important question: So, what are the options?

Well, one option might be to use Cloud Computing. There are several providers of this type of service. However, there are multiple issues to deal with. One most important concern is, how do we keep the IP safe. The others would be the amount of time it takes to upload and download potentially multiple terabytes of input and the final output data, and how to review intermediate results without incurring the significant cost of downloading the data that is generated.

The data transfer can be improved in various ways, e.g. through improved network bandwidth, compression, or, if the data is humongous, maybe even using couriers to shuttle hard drives back and forth. Reviewing results could be done via secure VPN connections. The problem of keeping IP secret is more problematic, and indeed is probably the major concern for this approach. So, how might this be addressed? One answer could be encryption. If the data to be processed is for example, PGP encrypted, no non-state entity, possibly not even government entities, should be able to decipher it. The software used to process the data would have to have the secret key encoded in a secure way, decrypt the data into memory, apply whatever processing is needed, and then re-encrypt the data before writing it back to disk.

Now, the vulnerability of data moves to the stage when it is being processed in memory. Decrypting and re-encrypting constitutes a computational overhead, but this may be acceptable, since I/O may be the bottleneck in most cases. Protecting the unencrypted data in memory could be managed by requiring servers to be secure, e.g. being re-imaged with a secure OS before use, dedicated to one client at a time, and run only necessary processes and protocols with access to dedicated ports. The remaining loopholes are human error and/or malicious acts. Either of these could occur anywhere, anytime, but proper training could minimize this risk. Additionally, one might choose to keep the most sensitive layers in house and only consider processing the remaining layers using Cloud Computing. Having pieces of data flow through multiple paths asynchronously can improve overall security and integrity.

In summary, depending on company resources, sensitivity of data and urgency of data processing, Cloud Computing could be a viable alternative for data processing from GB to TB to PB and beyond.

The sky may be the limit, with some dense Clouds helping us as we soar upwards …

BACUS

N • E • W • S

BACUS News is published monthly by SPIE for BACUS, the international technical group of SPIE dedicated to the advancement of photomask technology.

Managing Editor/Graphics Linda DeLano
Advertising Melissa Farlow
BACUS Technical Group Manager Marilyn Gorsuch

SPIE.

P.O. Box 10, Bellingham, WA 98227-0010 USA
Tel: +1 360 676 3290
Fax: +1 360 647 1445
www.SPIE.org
help@spie.org

Figure 2. The PROVE® mask qualification tool that was used in this work to determine the registration errors.

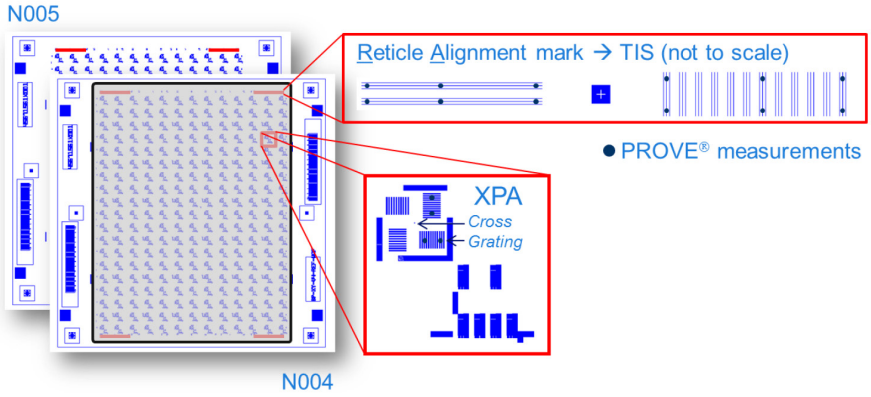

Figure 3. The 2 Baseliner masks that were used in this experiment. Both masks have identical layouts and contain metrology modules in a 13x19 layout. Mask N004 is equipped with a pellicle. PROVE® measurements were done on the locations indicated by the black dots. Both the XPA grating that can be read by the scanner alignment system and the reticle alignment marks (TIS marks) were read. N004 was measured on the PROVE® with and without pellicle frame mounted.

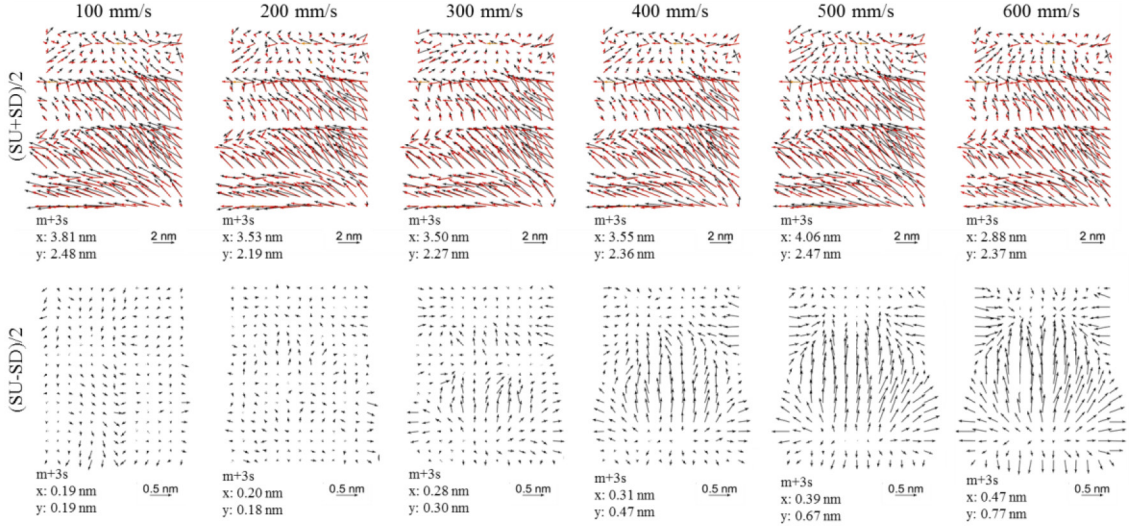

Figure 4. Top row: average intra-field overlay as function of scan speed. For all scan speeds, the reticle writing error difference between N004 and N005 dominates. When (SU-SD)/2 is plotted, all the static overlay contributors drop out and only the pellicle contribution remains. The dynamic pellicle contribution clearly increases with increasing scan speed.

correlation between offline mask-to-mask overlay measurements and on-wafer measurements *is* expected to deteriorate when *only one* of the masks is equipped with a pellicle. Evidence for this was already found even when we operated the scanner in slow scan mode.

In this work, we have extended the study by considering the impact of a pellicle on one of the masks and how it affects the intra-field overlay. As a logical consequence, it will have an impact on the correlation between the mask-to-mask and the on-wafer overlay measurements. An experimental technique has been developed to isolate the main impact of a scanning pellicle. We show that, in addition to the mask-to-mask writing errors, the pellicle induced errors can be characterized as well. We demonstrate that the correlation is restored when the pellicle contribution is removed from the on-wafer overlay measurements. The impact of the pellicle on the intra-field overlay performance should be treated as a separate overlay contributor that needs to be minimized separately. Calibration and scanner correction capabilities are in place to mitigate the pellicle induced overlay errors.

1. INTRODUCTION

The on-product overlay performance is no longer dominated by the scanner baseline overlay performance alone. It has been demonstrated that the NXT Dedicated Chuck Overlay performance can be as low as ~1-nm[1]. This performance level is getting close to the state-of-the art mask-to-mask writing error contribution[2, 3] that is measured on a relatively sparse sampling grid. The impact of a pellicle on the intra-field overlay performance can no longer be neglected either. When all critical layers are exposed on NXT immersion systems, the common errors introduced by a moving pellicle membrane drop out in the overlay. However, this is not the

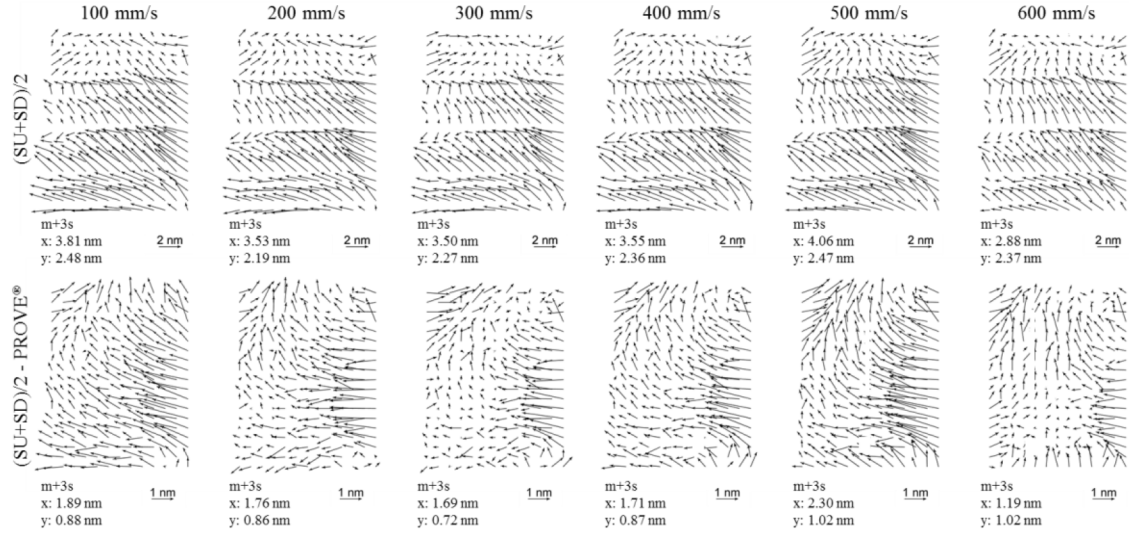

Figure 5. Top row: average scanner based intra-field overlay (SU+SD)/2 as function of scan speed. After removal of the mask-to-mask overlay as measured on the PROVE® tool, the bottom row remains.

case anymore when the first layer is exposed on an NXT system and the second layer is exposed on an NXE system (or vice versa). Since the latter is operated in vacuum, pellicle induced displacement errors are absent. This is not the case for the NXT system where the moving pellicle acts as a micro lens and introduces an additional overlay contribution in the matched machine overlay between an NXT and an NXE system.

In an earlier study, we demonstrated that the mask-to-mask overlay contribution as measured by the PROVE® registration tool correlates very well with the on-wafer overlay measurements[4]. The small mismatch of ~0.58-nm could be explained by a careful analysis of the underlying budget. The major contributors identified were the reticle alignment contribution and the difference in the way the registration measurements are performed by the scanner and PROVE® tool respectively.

The impact of a pellicle on the correlation between the off-line mask-to-mask measurements and the on-wafer results was considered as well. Therefore, one reticle was equipped with a pellicle. The pellicle introduced an additional penalty of ~0.4-nm in the mismatch. It should be noted that the exposures were performed at a slow scan speed of 100-mm/s.

We decided to extend the study by considering the on-wafer overlay at different scan speeds. The expectation is that the impact of the pellicle on the intra-field overlay will increase with increasing scan speeds. The goal of this paper is to consider the pellicle induced overlay penalties and the impact on the correlation with the mask-to-mask overlay as measured on an off-line registration tool. Although all experiments are performed on an immersion system, the learnings may also be applicable to match an NXT with an NXE system.

1.1 Pellicle membrane deflection during scan

A pellicle frame mounted on the reticle may result in an intra-field distortion that contains a static and a dynamic contribution. The static contribution consists of the actual mounting of the pellicle frame onto the quartz substrate in combination with the way the reticle is clamped on the reticle stage. This gives rise to a static intra-field distortion fingerprint. The dynamic contribution arises from the fact that the membrane is free to move. The positions are only fixed at locations where the membrane is attached to the supporting pellicle frame. On all other locations, the membrane is susceptible to pressure changes, vibration modes, and air flows. Figure 1 shows a schematic picture of a reticle while scanning. It should be noted that this is a very simplistic view of the reality, but it will help to explain the phenomena we observe later in the experiment.

The exposure sequence of the fields on an ASML TWINSCAN™ scanner is throughput optimized such that scan-up (SU) fields are alternated by scan-down (SD) fields. In case the scan properties for the SU and the SD fields are equal except for the (*y*) scanning direction, one may expect the pellicle deflection (D) and its induced intra-field overlay fingerprints to mirror with respect to the *xz*-plane if the scan direction is reversed, i.e. $D_{SU}(x,y) = D_{SD}(x,-y)$. As first approximation, it is also reasonable to assume that the pellicle deflection reproduces under a 180° rotation around the *x*-axis, i.e. $D(x,y) = -D(x,-y)$ and as a result $D_{SU}(x,y) = -D_{SD}(x,y)$. This means that the dynamic contribution of the pellicle membrane can be isolated in the (SU-SD)/2 overlay intra-field. Basically, the other (static) overlay contributors like the reticle stage clamping difference between the two masks and reticle writing error differences drop out since they are the same for the SU and SD fields.

However, when the average field or (SU+SD)/2 intra-field signature is considered, the static overlay contributors mentioned above remain. The dynamic contribution of the pellicle membrane to the overlay cancels in this case. It should be noted that the reticle writing error contribution including the distortion due to pellicle frame mounting can be characterized by an off-line mask registration tool like the PROVE®. This means that this part of the overlay contribution can be removed from the (SU+SD)/2 intra-field overlay signature. In the previous work, we did not observe a significant clamping difference when both masks were not equipped with a pellicle frame[4]. This can easily be understood by the fact that the two masks were identical by design. Since a pellicle frame is mounted on one of the masks, we cannot assume the masks are identical anymore.

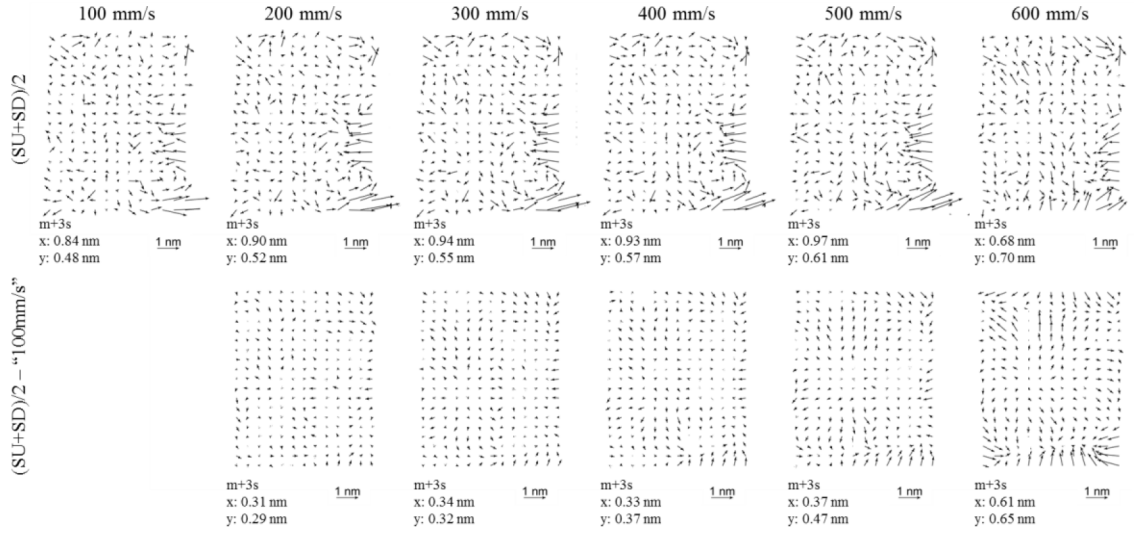

Figure 6. Top row: average scanner based intra-field overlay after removal of the mask-to-mask contribution and the linear terms as function of scan speed. A distinct fingerprint is present in the lower right area of the field. After removal field fingerprint at 100 mm/s from the remaining field fingerprints at higher scan speeds a small but growing fingerprint is observed.

The goal of this paper is to highlight the pellicle contribution as part of the total intra-field overlay signature. The reason is that when the pellicle-induced overlay penalties are ignored, the excellent correlation we found earlier between the offline determined mask-to-mask and the on-wafer determined overlay may not hold any longer. It should be noted that when all layers are exposed on NXT systems with reticles having the same pellicle type under the same scan conditions, the pellicle-induced errors will cancel and will not show up in the overlay. In case the pellicle types are different, the scan speed conditions are not the same, or when the pellicle-induced overlay penalty for one of the layers is absent (e.g. no pellicle or NXE), additional overlay penalties are expected.

In line with the earlier publication[4], we would like to treat the pellicle induced overlay penalty as a separate overlay contributor that needs to be addressed and solved separately. Currently, programs within ASML are in place to understand and solve these kind of overlay penalties in a structural way. The findings will be implemented in future ASML TWINSCAN™ systems. Alternatively, the ASML overlay optimizer products can be applied.

2. EXPERIMENTAL DETAILS

2.1 The PROVE® mask qualification tool

Figure 2 shows the PROVE® registration tool that was used for the registration and overlay measurements on mask level. The tool can be characterized by a unique combination of litho-grade optics, the DUV actinic wavelength (193-nm), the high detection NA, the superior stage concept with tight environmental control and sophisticated 2D correlation methods[5].

All masks that leave the mask shop are qualified by performing registration measurements to check if the pattern placement and mask-to-mask overlay is within specification. When the registration of the reticle alignment marks that are used by the ASML TWINSCAN™ systems (TIS or PARIS marks) are incorporated in the measurement scheme, the mask-to-mask overlay can be fully determined off-line. Since this can also be done when (one of) the masks is/are equipped with a pellicle, static pellicle frame induced overlay penalties can be characterized as well. A direct comparison with the on-wafer overlay can be made.

Although we consider only DUV masks in this study, PROVE® enables registration measurements on EUV masks as well[6]. This means that the correlation study between the off-line mask-to-mask and the on-wafer overlay can be extended to use-cases where both DUV and EUV masks are used.

In this study, we measured two DUV masks with PROVE® using the symmetry correlation mode and five successive measurement loops for each mask. After mounting a pellicle frame on one of the reticles, the PROVE® measurements were repeated. This was done on a different PROVE® tool. The locations where the registration measurements were performed are detailed out in the next section.

2.2 Scanner based mask-to-mask overlay measurements

For this investigation, two ASML BMMO (Baseliner Matched Machine Overlay) masks were ordered. The mask identification numbers are:

- 45671561N004 → EBM-6000
- 45671561N005 → EBM-5000

In the remainder of this paper we will refer to these masks by using N004 and N005. The masks were made on two different (older generation) e-beam writing tools, the EBM-6000[7] and the EBM-5000[8]. The initial scanner experiments and PROVE® measurements were performed without pellicles. After we collected and analyzed the data, N004 was equipped with pellicle 6ABLB-A2J from Shin-Etsu. The main results presented in this paper are obtained for the case where N004 is equipped with the pellicle and N005 is without a pellicle.

Figure 3 shows the layout of the N004 and N005 masks used. The N004 reticle contains a pellicle as shown in the figure. The masks under test contain TIS (Transmission Image Sensor) reticle alignment (RA) marks that were used to align the reticle. Metrology modules in a (13 x 19) layout are present inside the image field. One module is shown in an expanded view. It contains on-wafer overlay registration targets that can be measured with Yieldstar as well as marks (XPA) that can be read-out on the scanner. In this

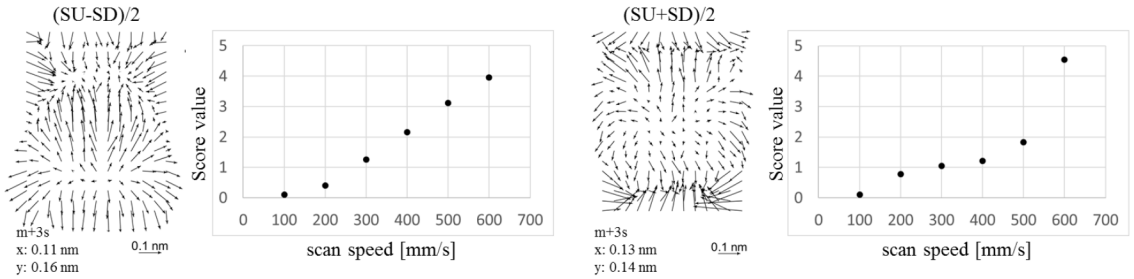

Figure 7. Pellicle induced overlay fingerprints as derived from a PCA on the (SU-SD)/2 and the (SU+SD)/2 intra-field overlay fingerprints. The magnitude of the fingerprint (score value) is shown in the two graphs next to the main fingerprints (or principal components).

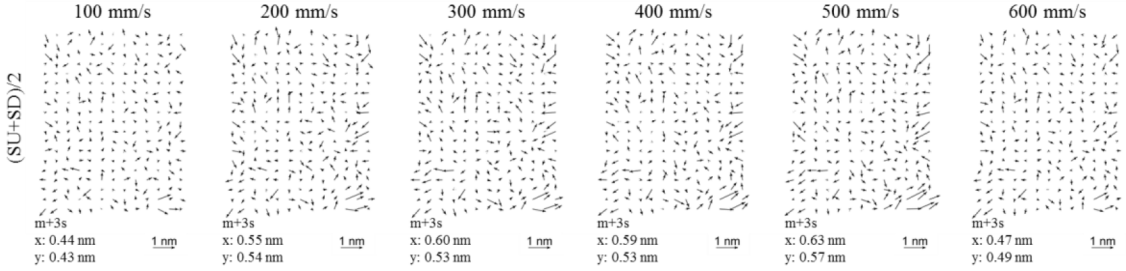

Figure 8. Average scanner based intra-field overlay (SU+SD)/2 after removal of the mask-to-mask contribution, the linear terms, the clamping difference between the two masks and the dynamic pellicle contribution as function of scan speed. The remaining field fingerprint is the same for all scan-speeds. The remaining fingerprint can be assigned to intra-grating variations in combination with the different measurement sampling of mask versus scanner wafer metrology.

work, we restrict ourselves to the XPA scanner read-out. PROVE® registration measurements were done at two locations inside each grating direction (*x* and *y*). It should be noted that only the grating areas are "seen" by the scanner. We decided to select two measurements per grating to improve the accuracy and to keep the total number of off-line registration measurements reasonable.

The way we extract the on-wafer overlay was extensively described in reference[4], to which we would like to refer the reader for all details. We did not deviate from that approach except that N004 is now equipped with a pellicle. All experiments were executed on the ASML NXT:1970Ci ($\leq$ 2-nm single machine overlay, dedicated chuck, full wafer coverage).

In the current work, the experiments were executed at 6 different scan speeds; 100-mm/s, 200-mm/s, 300-mm/s, 400-mm/s, 500-mm/s, and 600-mm/s enabling us to study the dynamic pellicle effect. The lowest scan-speed (100-mm/s) was used before in the previous work. We increased the scan-speed with steps of 100-mm/s to carefully investigate the increasing effect of the pellicle contribution on the intra-field overlay performance. All scan-speeds reported here are at wafer level, the scan speeds at reticle level are a factor of 4 higher.

This time, we have used 4 wafers to average out some of the reticle alignment contribution in the measured overlay. We know that this may still impact the accuracy when comparing the off-line determined mask-to-mask overlay with the on-wafer determined overlay, as was shown in reference[4]. Although all fields on the wafers were exposed (full wafer coverage), only the 12 selected fields were used for scanner overlay readout. These (4×3) fields were selected in 4 quadrants to ensure unambiguous wafer stage grid plate control. In addition, the exposure field scan direction was equally balanced resulting in 6 Scan-Up and 6 Scan-Down fields.

3. RESULTS

3.1 Isolation of the dynamic pellicle contribution: (SU-SD)/2

Figure 4 (top row) shows the average intra-field overlay fingerprint based on 12 fields per wafer as function of the scan speed at wafer level. As mentioned in the previous section, 4 wafers have been used per scan speed to average out some part of the reticle alignment contribution.

The average field is determined based on the *average* of the scan-up and scan-down fields (SU+SD)/2. In total, 6 scan-up and 6 scan-down fields were measured. This means that it is anticipated that the dynamic pellicle contribution in the average intra-field overlay fingerprint drops out. The red arrows represent the mask-to-mask overlay fingerprint as measured off-line on the PROVE®. This fingerprint is the same for all scanner scan speeds since the PROVE® measures the masks in static mode. The black arrows represent the scanner-based overlay measurements. Since the mask-to-mask registration errors are dominating the intra-field overlay performance, there is no obvious dependency on scan speed.

The pellicle contribution that changes with the scan direction can be highlighted by considering the (SU-SD)/2 intra-field fingerprint as function of the scan speed. All the static intra-field overlay contributors like the reticle writing error difference and clamping difference are the same for the SU and SD fields and consequently drop out. What remains is a clear pellicle fingerprint that grows in magnitude for increasing scan speeds. At 600 mm/s, the contribu-

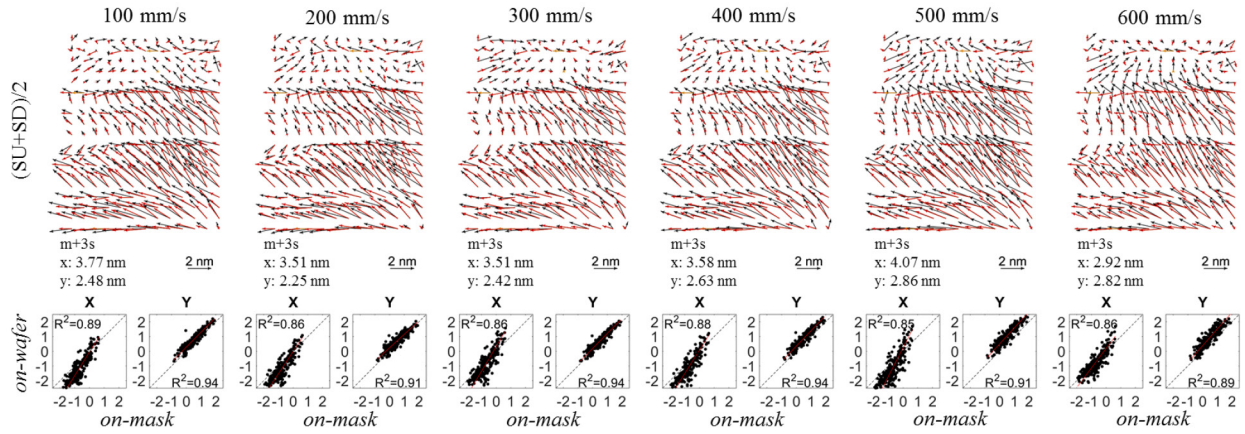

Figure 9. The mask-to-mask overlay as measured by PROVE® compared to the on-wafer results. The scan-up fields (SU) were considered only to see the full impact of the pellicle induced overlay distortion. The correlation plots between off-line determined mask-to-mask overlay and the on-wafer determined overlay are much worse compared to what was published before[4]. The root cause is that the on-wafer overlay is not only determined by the mask-to-mask registration errors.

tion is approximately 0.8-nm per scan direction.

In this section, we only mention that the growing fingerprint has been characterized by performing a principal component analysis (PCA) on the bottom row field fingerprints in Figure 4[9]. We come back to it in the next section. It enables us to remove the scanning pellicle contribution from the measured overlay of the SU and SD fields.

3.2 Remaining intra-field overlay contributors: (SU+SD)/2

In this section, we would like to consider the different overlay contributors that determine the average field overlay performance more closely. In Figure 5, the on-wafer measured intra-field overlay is shown as function of the scan-speed (top row). As mentioned before, the intra-field overlay is dominated by the reticle writing error difference between the two masks. Since the mask-to-mask overlay contribution can be accurately determined off-line by PROVE®, we can safely remove this contribution from the measured average field fingerprints. The results are also shown in Figure 5 (bottom row field plots). Note that the scale of the bottom row has been decreased to 1-nm to reveal the underlying fingerprint. There is some commonality observed in the field fingerprints that are obtained at different scan speeds. The average field fingerprint seems to contain linear terms as well as higher order terms.

At this level of the analysis, we attribute this intra-field fingerprint to the reticle clamping difference between N004 and N005 and a residual reticle alignment contribution. Since we used TIS reticle alignment, it only affects the linear terms. In the previous publication on this topic, we concluded that even 10 wafers were not sufficient to fully average out the reticle alignment contribution. A residual penalty of approximately 0.4-nm remained. This time, we have used only 4 wafers per scan speed. Therefore, we decided to remove the linear terms from the bottom row field fingerprints as well to reveal the higher order overlay signature. We realize that the reticle clamping contribution may contain linear terms as well. This contribution can only be isolated by measuring and averaging more wafers.

The top row field plots in Figure 6 show the results after removal of the linear terms from the bottom row field plots from Figure 5. A distinct higher order distortion fingerprint is present in the lower right-hand side of the field. We attribute this local distortion fingerprint to the difference in clamping behavior of N004 (with pellicle frame) and N005 (without pellicle frame). At this moment in time it is not clear whether this observation is linked to the mounting procedure of the pellicle under study or whether it is more generally applicable. It should be noted that this distinct fingerprint was not observed when the overlay was measured for these masks without pellicles.

Although the remaining fingerprints look very similar for the different scan speeds, we decided to do a final check on the variation across the scan speeds. To that end, the fingerprint at 100 mm/s is removed from the remaining fingerprints. The result is also shown in Figure 6 (bottom row). A small but noticeable increasing fingerprint is observed. Although the penalty is small for scan speeds up to 500-mm/s, the magnitude increases for 600-mm/s. This means that the pellicle deflection and its resulting overlay fingerprint do not exactly fulfill the condition $D_{SU}(x,y) = -D_{SD}(x,y)$ for the highest scan speed we investigated. It seems that a new mode of the pellicle membrane gets more dominant in the intra-field overlay for higher scan speeds.

We attribute this new mode to the dynamic pellicle contribution as well. Also, in this case, a PCA was performed to characterize this fingerprint. When we combine the PCA from the previous section and this section, two dominant field fingerprints due to the dynamic pellicle fingerprint can be extracted. The results are summarized in Figure 7.

The first pellicle induced fingerprint that was obtained from the (SU-SD)/2 analysis as function of the scan speed (Figure 4, bottom row) and is shown on the left-hand side in Figure 7. It almost linearly grows with increasing scan speed. This fingerprint is *not* present in the average intra-field overlay (SU+SD)/2 but it is present when the overlay is analyzed for the SU and SD fields separately.

The second pellicle induced fingerprint was extracted from the (SU+SD)/2 analysis (Figure 6, bottom row). Its magnitude seems to increase more rapidly for the highest scan speed investigated in this study. The fact that this fingerprint exists implies that the pellicle induced overlay fingerprint is not exactly meeting the conditions we set in section 1.1 and that the impact of the pellicle on the intra-field overlay is more complex than was outlined in that section. However, we have shown that the pellicle induced intra-field overlay penalties can be characterized experimentally.

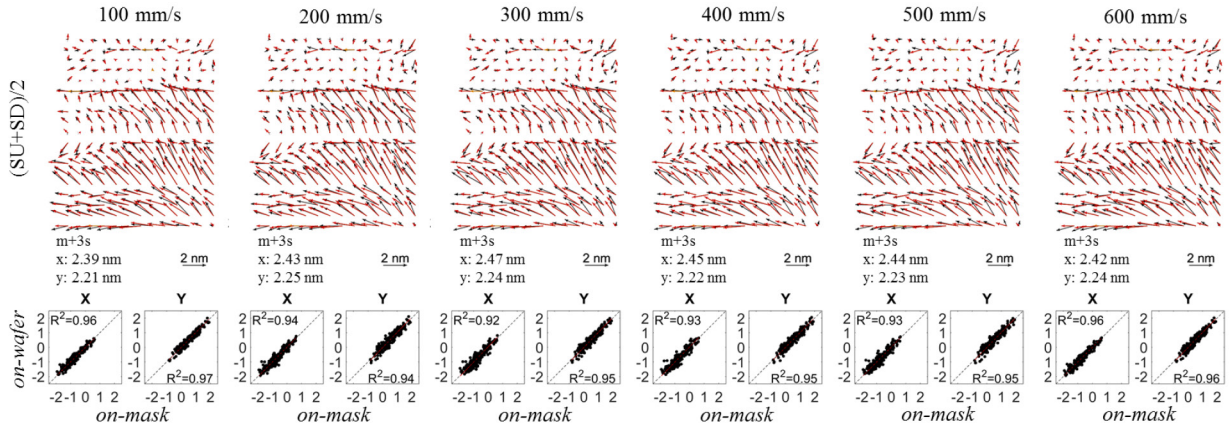

Figure 10. The mask-to-mask overlay as measured by PROVE® compared to the on-wafer results. The pellicle induced overlay penalties and the static reticle-to-reticle clamping difference are removed from the on-wafer overlay measurements. The correlation is restored to the levels when both masks were still without a pellicle (R^2 ~0.96).

This means we can still correct the measured intra-field overlay for the pellicle induced penalties.

In Figure 8, we show the result when *both* the higher order clamping difference *and* the (second) pellicle induced fingerprint is removed from the top row field plots presented in Figure 6. The remaining field fingerprint is independent of the scan speed and close to the intra-grating sampling difference between the PROVE® and the scanner overlay readings as we observed earlier. We consider this to be the baseline of the experiment.

3.3 Impact on mask-to-mask and on-wafer overlay correlation

In this section, we would like to consider the impact of the additional overlay contributors when one of the mask is equipped with a pellicle on the correlation between the mask-to-mask overlay as determined by an off-line measurement tool like the PROVE® and the on-wafer measured intra-field overlay. In case the comparison is made based on the average measured field (SU+SD)/2, part of the dynamic pellicle contribution cancels. Therefore, we decided to show the correlation by considering one of the scan directions only. The full pellicle induced overlay penalty is present when SU or SD field are considered individually. In this paper we will demonstrate the correlation results for the SU fields only. We could have chosen the SD fields as well. The results are very similar.

In Figure 9, the correlation results are shown for the mask-to-mask overlay as measured by the PROVE® (in red) and the overlay results as measured on the scanner for the SU fields only. As discussed in the previous two sections, the on-wafer intra-field overlay is built-up of three sub-contributors: the mask-to-mask reticle writing error contribution, the dynamic pellicle induced overlay contribution, and the reticle clamping contribution. All these contributors have been identified separately. If we consider the point-to-point correlation plots between the off-line determined mask-to-mask overlay and the on-wafer SU overlay, the results are deteriorated compared to what was published earlier[4]. The R^2 values dropped down from 0.96 previously to 0.85 in *x* and 0.89 in *y* (worst values), respectively. In addition, the slope (especially in *x*) deviates from 1 and there is an offset observed for y. The correlation is still present since the reticle writing error contribution is dominating the intra-field overlay. In case the masks would have been written on high-end e-beam systems for which the reticle writing error contribution is significantly smaller, one may erroneously conclude that there is no correlation between the off-line determined mask-to-mask overlay and the on-wafer measured overlay.

Since we have identified all the individual overlay contributors separately, they can be removed from the on-wafer measured results. The pellicle induced penalties for the different scan speeds could be characterized by the fixed intrafield fingerprint times a score value as was shown in Figure 7. The reticle-to-reticle clamping contribution is constant for different scan speeds. This is of course according expectation since the masks are first clamped on the reticle stage before the exposures in scanning mode take place.

In Figure 10 the correlation plots are shown after removal of the additional overlay contributors. The correlation between the on-wafer measured overlay and the off-line determined mask-to-mask overlay is fully restored. The R^2 values of around 0.96 are independent of scan speed. These values are identical to the value obtained earlier when both masks were still without with a pellicle[4]. The correlation slope is close to one and point-to-point residuals are equal to or less than 0.63-nm, see also Figure 8. This implies that the mask-to-mask overlay contribution can be determined by an offline tool and used for Feed-Forward control to the scanner.

4. DISCUSSION

The impact of a pellicle mounted on a mask on the intra-field overlay cannot be neglected anymore. It was demonstrated recently that the contribution of the pellicle alone can be as large as 1.8-nm[1]. In this work, the pellicle induced overlay has been characterized on 24 wafers in total: 6 different scan speeds times 4 wafers per scan speed. The maximum pellicle induced penalty per fingerprint is ~0.6-nm at 600-mm/s, see Figure 7. However, the ASML NXT:1970Ci normally operates at a scan speed of 800-mm/s. In case we extrapolate the values as shown in Figure 7 to a scan speed of 800-mm/s, pellicle induced penalties of 1.0-nm to 1.3-nm are obtained. These numbers come already closer to 1.8-nm which is comparable to the baseline performance of the ASML NXT:1970Ci (≤ 2-nm single machine overlay, dedicated chuck, full wafer coverage).

The isolated pellicle induced distortion penalty is surprisingly large. However, it should be realized that we investigated the worst-case scenario one mask was equipped with a pellicle and the other one was not. In a production environment, all masks contain

a pellicle and the common pellicle induced distortion penalties are cancelled when the layer-to-layer overlay is considered. This assumes that the pellicle type and scan speeds are the same for the different layers. This is not necessarily true when the scanners operate at different scan speeds and/or when NXT to NXE matching is concerned.

The results we presented in this paper cannot be generalized to all available pellicles. Different pellicle types have different properties. The current recommendation is to use pellicle frames with a low stand-off height (~3-mm), thin membrane thickness (280-nm), and high pre-stress (> 7.5-MPa)[1]. The pellicle we used in this investigation has a stand-off height of 3.5-mm, a membrane thickness of 280-nm, and a moderate pre-stress of around 5.0-MPa.

In line with previous work, we consider the total on-wafer overlay as the sum of individual contributors that should be characterized and optimized separately. This is also true for the pellicle induced overlay penalty. Overlay penalties can be mitigated by selecting a pellicle frame according to the current recommendations and/or by applying appropriate scanner exposure corrections[1]. The reduction and/or elimination of the pellicle induced overlay penalties is beyond the scope of this paper. We only would like to create awareness that these additional overlay penalties deteriorate the correlation between the off-line determined mask-to-mask overlay and the on-wafer measured overlay.

5. CONCLUSIONS

Additional intra-field overlay contributors will become part of the measured scanner overlay performance when one of the two masks used is equipped with a pellicle. The presence of a pellicle (frame) can introduce two additional overlay signatures. The first one is a direct result of the deflection of the pellicle membrane during scan. The membrane acts as a micro lens causing pattern displacements. When a pellicle (frame) is mounted onto a reticle, it makes it a physically different reticle than when it was still without a pellicle (frame). As a result, the reticle stage clamping performance may change compared to the case where the two masks were both without pellicles.

We have analyzed the intra-field overlay performance for different exposure scan speeds for the use-case when there is one mask with and the other one without a pellicle. This enabled us to isolate the underlying overlay contributors. Although the experiments were performed on a DUV scanner, the learnings can be applied for the DUV-EUV matching use-case as well. The correlation between off-line mask-to-mask measurements and on-wafer measurements is deteriorated when the presence of additional overlay contributors is not taken care of. The correlation can even be lost if the ratio between the mask-to-mask writing errors and the additional intra-field overlay contributors becomes smaller. This may happen when both masks are created on a high-end e-beam writer. It could lead to the *wrong* conclusion that there is no correlation between off-line mask-to-mask registration measurements and the on-wafer determined overlay measurements.

In this paper, we have demonstrated that the correlation between the off-line determined mask-to-mask overlay as measured on the PROVE® and the on-wafer intra-field is fully restored after removal of the additional (known) overlay contributors. The additional overlay contributors are introduced since one of the reticles contains a pellicle (frame). This leads us to the main conclusion of this work: the strong correlation between the off-line determined mask-to-mask overlay and the on-wafer results is still present provided that the additional overlay contributors are not present or eliminated. This implies that the off-line determined mask-to-mask overlay fingerprint can be used to apply corrections on the scanner during exposure or on a mask modification tool.

6. REFERENCES

[1] Theo Thijssen, Marcel Beckers, Albert Mollema, Leon Levasier, and Alexander Padi, et al., “Cross-platform (NXENXT) machine-to-machine overlay matching supporting next node chip manufacturing,” **Proc. of SPIE Vol. 10587,** 1058709 (2018).

[2] Hideki Matsui, Takashi Kamikubo, Satoshi Nakahashi, Haruyuki Nomura, Noriaki Nakayamada, Mizuna Suganuma, Yasuo Kato, Jun Yashima, Victor Katsap, Kenichi Saito, Ryoei Kobayashi, Nobuo Miyamoto, and Munehiro Ogasawara, “Electron beam mask writer EBM-9500 for logic 7nm node generation,” **Proc. of SPIE Vol. 9985,** 998508 (2016).

[3] Hiroshi Matsumoto, Hiroshi Yamashita, Takao Tamura, and Kenji Ohtoshi, “Multi-beam mask writer MBM-1000,” **Proc. of SPIE Vol. 10454,** 104540E (2017).

[4] Richard van Haren, Steffen Steinert, Christian Roelofs, Orion Mouraille, Koen D’havé, Leon van Dijk, and Dirk Beyer, “Off-line mask-to-mask registration characterization as enabler for computational overlay,” **Proc. of SPIE Vol. 10451,** 1045111 (2017).

[5] Dirk Seidel, Michael Arnz, and Dirk Beyer, “In-die photomask registration and overlay metrology with PROVE using 2D correlation methods”, **Proc. of SPIE Vol. 8166** (2011).

[6] Steffen Steinert, Hans-Michael Solowan, Jinback Park, Hakseung Han, Dirk Beyer, and Thomas Scherübl, “Registration performance on EUV masks using high-resolution registration metrology”, **Proc. of SPIE Vol. 9985** (2016).

[7] Jun Yashima, Kenji Ohtoshi, Noriaki Nakayamada, Hirohito Anze, Takehiko Katsumata, Tomohiro Iijima, Rieko Nishimura, Syuuichiro Fukutome, Nobuo Miyamoto, Seiji Wake, Yusuke Sakai, Shinji Sakamoto, Shigehiro Hara, Hitoshi Higurashi, Kiyoshi Hattori, Kenichi Saito, Rodney Kendall, and Shuichi Tamamushi, “Electron-beam mask writer EBM-6000 for 45 nm HP node”, **Proc. of SPIE Vol. 6607,** 660703-1 (2007).

[8] Hitoshi Sunaoshi, Yuichi Tachikawa, Hitoshi Higurashi, Tomohiro Iijima, Junichi Suzuki, Takashi Kamikubo, Kenji Ohtoshi, Hirohito Anze, Takehiko Katsumata, Noriaki Nakayamada, Shigehiro Hara, Shuichi Tamamushi, and Yoji Ogawa, “EBM-5000: Electron beam mask writer for 45 nm node”, **Proc. of SPIE Vol. 6283,** 628306-1 (2006).

[9] Trevor Hastie, Robert Tibshirani, and Jerome Friedman, “The Elements of Statistical Learning: Data Mining, Inference, and Prediction”, Springer (2009).

BACUS N • E • W • S

Sponsorship Opportunities

Sign up now for the best sponsorship opportunities

Photomask 2018 —
Contact: Melissa Farlow,
Tel: +1 360 685 5596; **melissaf@spie.org**

Advanced Lithography 2018 —
Contact: Teresa Roles-Meier,
Tel: +1 360 685 5445; **teresar@spie.org**

Advertise in the BACUS News!

The BACUS Newsletter is the premier publication serving the photomask industry. For information on how to advertise, contact:

Melissa Farlow,
Tel: +1 360 685 5596
melissaf@spie.org

BACUS Corporate Members

Acuphase Inc.
American Coating Technologies LLC
AMETEK Precitech, Inc.
Berliner Glas KGaA Herbert Kubatz GmbH & Co.
FUJIFILM Electronic Materials U.S.A., Inc.
Gudeng Precision Industrial Co., Ltd.
Halocarbon Products
HamaTech APE GmbH & Co. KG
Hitachi High Technologies America, Inc.
JEOL USA Inc.
Mentor Graphics Corp.
Molecular Imprints, Inc.
Panavision Federal Systems, LLC
Profilocolore Srl
Raytheon ELCAN Optical Technologies
XYALIS

Industry Briefs

WSTS Raises Chip Sales Forecast

Dylan McGrath

SAN FRANCISCO — The global semiconductor market will grow by 12.4 percent in 2018, reaching $463 billion, according to the latest forecast from World Semiconductor Trade Statistics, an organization of more than 55 chip suppliers that pools sales data.

The latest forecast is more bullish than the original WSTS forecast for 2018, issued last November. That forecast called for chip sales to increase by 7 percent. Sales are expected to increase across all product categories and in all regions of the world.

WSTS said it raised the chip sales forecast based on continued extraordinary growth in the memory segment as well as strong growth in analog chips. Those two markets are expected to grow by 26.5 percent and 9.5 percent, respectively, this year.

The forecast calls for sales to increase by a furter 4.4 percent in 2019, reaching $484 billion.

https://www.eetimes.com/document.asp?doc_id=1333357

What's In A Node?

The time has come to shift to a new taxonomy in which materials and 3D techniques are included.

SUNDEEP BAJIKAR

In an environment where process nodes are no longer consistently delivering the level of improvements predicted by Moore's Law, the industry will continue to develop "inter-nodes" as a way to deliver incremental improvements in lieu of "full-nodes." A shift in market requirements, in part due to the rise of AI and IoT, is increasing emphasis on trailing-nodes. When it comes to leading-nodes, while EUV offers improvements in resolution, it offers only a partial solution to layer-to-layer alignment errors (i.e. overlay errors or edge placement errors – EPE). Materials engineering is needed across the spectrum of nodes, to address layer-to-layer alignment through self-aligned structures in leading-nodes, help enable inter-nodes, as well as enhance trailing-nodes.

https://semiengineering.com/whats-in-a-node/

EUV in Final Push into Fabs Making progress amid 'a lot of pressure'

Rick Merritt

ANTWERP, Belgium — A 20-year struggle to launch a next-generation lithography tool has entered its final phase as engineers race to unravel a rat's nest of related issues. Despite complex problems and short deadlines to bring extreme ultraviolet (EUV) steppers into high-volume manufacturing, experts remain upbeat.

The good news is that many shoulders are pushing the wheel ahead. "In the past, one company would take a lead with a new semiconductor technology, but now all the logic guys are jumping in, biting the bullet, and taking the risks," said An Steegen, executive vice president of technology and systems at Imec.

https://www.eetimes.com/document.asp?doc_id=1333326

EUV Lithography: Extending the Patterning Roadmap to 3nm

Debra Vogler

This year's Advanced Lithography TechXPOT at SEMICON West will explore the progress on extreme ultra-violet lithography (EUVL) and its economic viability for high-volume manufacturing (HVM), as well as other lithography solutions that can address the march to 5nm and onward to 3nm. Several session speakers offered their insights into the readiness of EUVL for 5nm and how other lithography solutions will enable 3nm. See the full list of speakers and program agenda at http://www.semiconwest.org/programs-catalog/lithography-5nm-and-below.

http://blog.semi.org/semi-news/ultra-violet-lithography-extending-the-patterning-roadmap-to-3nm

IC Capex Projected to Top $100 Billion

Dylan McGrath

SAN FRANCISCO — Semiconductor industry capital spending is now expected to increase by 14 percent in 2018, pushing it above the $100 billion mark for the first time, according to a revised forecast by IC Insights. The market research firm had said in March it expected capital spending to increase by 8 percent this year.

Total semiconductor industry capital spending is now expected to be about $104 billion this year, 53 percent higher than the $68 billion that the industry shelled out in capital spending just two years ago in 2016, IC Insights (Scottsdale, Ariz.) said.

IC Insights attributed the increase largely to South Korean chipmakers Samsung Electronics and SK Hynix, which continue to enjoy the spoils of a seller's market for both DRAM and NAND flash memory.

https://www.eetimes.com/document.asp?doc_id=1333320

Join the premier professional organization for mask makers and mask users!

About the BACUS Group

Founded in 1980 by a group of chrome blank users wanting a single voice to interact with suppliers, BACUS has grown to become the largest and most widely known forum for the exchange of technical information of interest to photomask and reticle makers. BACUS joined SPIE in January of 1991 to expand the exchange of information with mask makers around the world.

The group sponsors an informative monthly meeting and newsletter, BACUS News. The BACUS annual Photomask Technology Symposium covers photomask technology, photomask processes, lithography, materials and resists, phase shift masks, inspection and repair, metrology, and quality and manufacturing management.

Individual Membership Benefits include:

- Subscription to BACUS News (monthly)
- Eligibility to hold office on BACUS Steering Committee

www.spie.org/bacushome

Corporate Membership Benefits include:

- 3-10 Voting Members in the SPIE General Membership, depending on tier level
- Subscription to BACUS News (monthly)
- One online SPIE Journal Subscription
- Listed as a Corporate Member in the BACUS Monthly Newsletter

www.spie.org/bacushome

CALENDAR

2018

SPIE Photomask Technology + EUV Lithography
17-20 September 2018
Monterey Convention Center
Monterey, California
www.spie.org/puv

2019

Photomask Japan
16-18 April 2019
PACIFICO Yokohama
Yokohama, Japan
www.photomask-japan.org

SPIE is the international society for optics and photonics, an educational not-for-profit organization founded in 1955 to advance light-based science, engineering, and technology. The Society serves nearly 264,000 constituents from 166 countries, offering conferences and their published proceedings, continuing education, books, journals, and the SPIE Digital Library in support of interdisciplinary information exchange, professional networking, and patent precedent. SPIE provided more than $4 million in support of education and outreach programs in 2017. **www.spie.org**

SPIE.
International Headquarters
P.O. Box 10, Bellingham, WA 98227-0010 USA
Tel: +1 360 676 3290
Fax: +1 360 647 1445
help@spie.org • **www.SPIE.org**

Shipping Address
1000 20th St., Bellingham, WA 98225-6705 USA

Managed by SPIE Europe
2 Alexandra Gate, Ffordd Pengam, Cardiff,
CF24 2SA, UK
Tel: +44 29 2089 4747
Fax: +44 29 2089 4750
spieeurope@spieeurope.org • **www.spieeurope.org**

You are invited to submit events of interest for this calendar. Please send to lindad@spie.org; alternatively, email or fax to SPIE.